

# Scalable and Modular Control Framework for Managing Active Cell Balancing Challenges

Afaq Ahmed, Ali Arshad Uppal, *Senior Member, IEEE*, and Qadeer Ahmed, *Senior Member, IEEE*

**Abstract**— Active cell balancing (ACB) is an important paradigm in an electric vehicle’s (EV) battery pack. However, in designing the ACB network (ACBN), the interconnections among cells and the selection of power electronic components lead to large variations. Therefore, to evaluate the performance of these diversifications, a modular and scalable framework is required. Consequently, this work utilizes graph theory to model and evaluate the ACBN performance for EV range extension. In this respect, a buck-boost (BB) converter-based architecture, which comprises  $N$  series adjacent cells, is modeled using the multiplex ( $\mathcal{M}$ )—a variant of a graph. Moreover, the high-fidelity expressions for balancing currents are integrated with  $\mathcal{M}$ . Building on that, a nonlinear model predictive control (NMPC) is formulated and subsequently solved to perform ACB. Similarly, the stability argument for the NMPC based on  $N$  cells is provided, and the provision to perform ACB for various ACBN types under the graph-NMPC-based framework is discussed. The simulations are performed for various real-life driving scenarios, and the results demonstrate that the BB converter-based architecture has been able to extend the average EV range up to 32 km under NMPC-based balancing.

**Index Terms**— Active cell balancing control, graph-based modeling, EV range anxiety and nonlinear model predictive control.

## I. INTRODUCTION

Cell balancing of an electric vehicle’s (EV) battery pack yields multiple advantages, such as improved battery health, longevity, and increased EV range. In this regard, active cell balancing (ACB) is a favored approach, as it prevents unnecessary energy loss. Moreover, the construction of an ACB network (ACBN) requires the selection of power electronic components and determining the charge transfer paths among the cells. These design decisions ultimately determine the performance of ACBN in terms of balancing time, power losses, battery health, and EV’s range, among others. Consequently, to evaluate the performance metrics achieved by various ACBN configurations, a mathematical framework is required that is both modular and scalable.

In broader terms, variations in ACBN can be classified based on the charge transfer topology and the power electronic com-

ponents, i.e., architecture [1]. Moreover, topologies can further be categorized based on whether balancing occurs between adjacent or non-adjacent cells. For instance, [2] provided a balancing framework for series, module, and layer-based adjacent topologies. Similarly, in the case of non-adjacent cells, balancing can be performed by employing cell-to-pack (C2P), pack-to-cell (P2C), module-based cell-pack, etc. [3]. From the balancing architecture’s standpoint, the common examples are the switching capacitor, buck-boost converter, and flyback converter [4].

To evaluate the efficacy of ACBN variants, different modeling approaches exist. For instance, in the system-theoretic approach, the balancing network is analyzed at the broader level, and the complexity of individual components is minimized [5]. On the other hand, computer software such as Simscape, PSpice, etc., is usually utilized to better capture the physics at the component level [6]. The system-level models are mostly based on differential equations (DE) and state-space models. Consequently, to add an element of physics at the component level, algebraic expressions are coupled with DE models to mimic the ACBN averaging behavior [7]. For instance, [8] provided average balancing currents expressions for inductor-based ACBN during charging and discharging scenarios. Moreover, graph theory (GT) has also been utilized in modeling and control of ACBNs [9]–[11]. In this regard, [12] provided a comprehensive framework to model the various charge transfer paths using the hypergraphs.

Similarly, various control techniques with increased focus on model predictive control (MPC) have been observed in the ACB paradigm [13]. Non-linear MPC (NMPC) has also been used to demonstrate EV’s range extension [14]. Moreover, different MPC variants in terms of cost functions in the face of different driving scenarios have been analyzed by [15].

It is obvious from the literature review that DE and its augmentation with algebraic expressions is a conventional approach in analyzing different ACBNs. However, this is usually done on an ad hoc basis. In this respect, the graph-based approach offers a modular (i.e., seamlessly captures any balancing topology) and scalable framework. However, to the best of the author’s knowledge, there is no study that simultaneously integrates GT and algebraic models to capture physics at the component level. This synergistic approach is further substantiated by our earlier work [16], wherein we demonstrated that considering static and dynamic parameters in ACBN is crucial in evaluating its performance. Therefore, in light of the above gap, this work aims towards the

The paper was submitted for review on September 12, 2025.

Afaq Ahmed and Ali Arshad Uppal are with the department of Electrical & Computer Engineering, COMSATS University Islamabad, Islamabad, Pakistan (e-mail: ali.arshad@comsats.edu.pk).

Qadeer Ahmed is with the department of Mechanical & Aerospace Engineering, The Ohio State University, Columbus, OH, USA (email: ahmed.358@osu.edu).

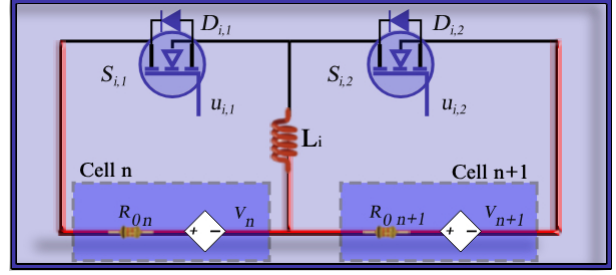
following contributions: (i) Proposing a modular modeling approach for ACBN variants using the multiplex graphs and integrating high-fidelity currents and detailed derivation of adjacent-based cell-cell ACBN for  $N$  cells. (ii) Formulating an NMPC problem encapsulating any cell connection and its subsequent solution for ACB, along with its stability argument. (iii) Demonstration of EV's range extension against real-world driving scenarios as a result of (i) and (ii).

The rest of the letter is distributed as follows: In Section II, the detailed modeling of the BB converter-based ACBN based on the graph structure is provided; similarly, in Section III, the NMPC problem is formulated for the ACBN containing  $N$  cells, and its subsequent stability is proved. Section IV provides the results on EV's range extension, and the letter is concluded in Section V.

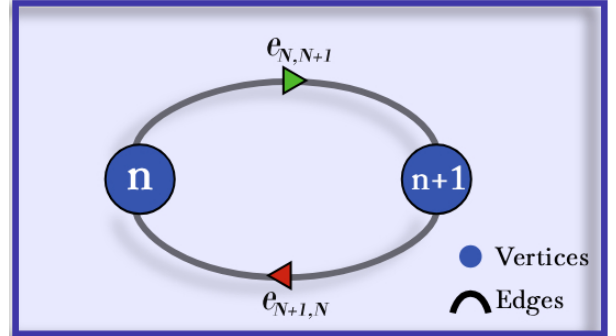
## II. GRAPH-BASED MODULAR AND SCALABLE MODELING OF ACTIVE CELL BALANCING NETWORK

Formally, a graph ( $\mathcal{G}$ ) is a pair of sets  $(V, E)$ , where  $V$  is a set containing vertices s.t  $V = \{v_1, v_2, \dots, v_N\}$  and  $E$  contain edges s.t  $E = \{e_{ij} \mid \forall i, j \in V\}$ . The adjacency matrix ( $\mathcal{A}$ ) of a  $\mathcal{G}$  is a  $|V| \times |V|$  matrix such that  $\mathcal{A}(i, j) = 1$  if there is an edge between vertices  $i$  and  $j$ , and  $\mathcal{A}(i, j) = 0$  otherwise. It can be seen that  $\mathcal{A}$  is particularly useful in encoding the information of cells' interconnections. This will become more concrete by modeling a BB converter-based architecture containing  $N$  serially connected cells. Moreover, the provision to incorporate other topologies using  $\mathcal{A}$  will also be discussed.

Figure 1a depicts the atomic unit for the BB-based converter. The atomic unit can be extended to  $N$  cells by simply replicating it  $N - 1$  times. Moreover, charge transfer or balancing in Figure 1a occurs using the following mechanism: cell  $n$  transfers charge to  $n + 1$  by activating Metal–Oxide–Semiconductor Field-Effect Transistor (MOSFET)  $S_{i,1}$ , which temporarily stores energy in inductor ( $L_i$ ). When,  $S_{i,1}$  and  $S_{i,2}$  are turned off, the energy flows from  $L_i$  to cell  $n + 1$ . The same principle holds in the case of cell  $n + 1$  transferring charge to  $n$ , but with the opposite order of switches. Similarly, Figure 1b represents the abstraction of ACBN in terms of graph. Therein the cells are represented as vertices, and the components in the charge transfer path are lumped into edges. The rationale behind this simplification is that since we have assumed a mean balancing current approach to model ACBN, this means charge usually transfers among cells at a rapid rate throughout the repeated cycles; however, when balanced by the currents, the net charge transfer within a single switching cycle is substantially lower than the charge stored within the cells. Consequently, the ACBN depicted in Figure 1 can be defined in terms of a graph as follows:  $\mathcal{G} = (V, E)$ , where  $V = \{v_1, v_2, \dots, v_N\}$  is the set of  $N$  vertices (cells); and  $E = \{e_{ij} \mid i \neq j, \text{ and } j = \{i \pm 1\}, \forall i, j \in V\}$  is the set of directed edges representing the charge transfer paths between adjacent cells. This graph can also be defined as  $\mathcal{G}_{ch}^1 = (V, E_{ch}^1)$ —the particular index notation will be clarified in the subsequent paragraphs. Similarly,  $\mathcal{A}(\mathcal{G})_{ch}^1$  represents the charge transfer network as an  $N \times N$  matrix:



(a) Building block for BB converter-based ACBN



(b) Building block for graph-based ACBN

Fig. 1: Atomic Unit for two representations of ACBN

$$\mathcal{A}(\mathcal{G})_{ch}^1(ij) = \delta_{i,j+1} + \delta_{i,j-1}, \quad \text{for } i, j \in \{1, 2, \dots, N\} \quad (1)$$

where  $\delta$  is the Kronecker delta function. In (1), setting  $N$  to any positive integer will yield a matrix containing information for interconnection of  $N$  cells, which demonstrates that the framework is easily scalable. Moreover, just by placing 1 in the  $(i, j)$  index of the adjacency matrix, a charge transfer path can be formed between cells  $i$  and  $j$  in a modular fashion. Moreover, connections in other topologies such as C2P/P2C, etc., can also be captured in the same manner. In C2P/P2C a vertex  $v_i$  can also represent a whole pack, wherein the state of charge (SoC) of  $v_i$  is the average SoC of the pack.

However, as illustrated in our previous work [16], the charging and discharging paths in Figure 1a have different expressions due to different physical parameters; thus,  $\mathcal{G}_{ch}^1$  alone can't accommodate these different paths. Consequently, we invoke the notion of multiplex, which is a family of graphs cascaded together such that  $\mathcal{M} = [\mathcal{G}^1, \dots, \mathcal{G}^l]$ , where  $l$  denotes the total number of layers—see Figure 2. Moreover, each  $\mathcal{G}^l$  is defined over the same set  $V$  and is given as  $\mathcal{G}^l = (V, E^l)$ . Consequently, to model our ACBN, we set  $l = 2$ ; this results in two graphs each for the charging and discharging paths. The graph for charging path is defined as:  $\mathcal{G}_{ch}^1 = (V, E_{ch}^1)$ ; whereas the graph for the discharging path  $\mathcal{G}_{dis}^2 = (V, E_{dis}^2)$  is set by taking the transpose of  $\mathcal{A}(\mathcal{G})_{ch}^1$  in (1).

Moreover, it can be observed in Figure 2 that weights  $w_{i,j}^{ch}/w_{i,j}^{dis}$  are assigned to the edges of each  $\mathcal{G}^l$ . The edges  $e_{ij}$  depicted in Figure 1b denote the physical connection between the cells/vertices, whereas  $w_{i,j}^{ch}/w_{i,j}^{dis}$  represent the control efforts or MOSFETs' duty cycles. Subsequently, there is a one-to-one mapping between  $w_{i,j}^{ch}/w_{i,j}^{dis}$  and  $e_{ij}$ , however

they both represent different things. Moreover,  $w_{i,j}^{ch}$  and  $w_{i,j}^{dis}$  are complementary in nature: NMPC only needs to compute either one of them. This, along with the fact that  $\mathcal{M}$  is defined over the same  $V$ , does not introduce additional computational burden on NMPC. Similarly, following convention regarding the current's direction in  $\mathcal{M}$  is adopted: in  $\mathcal{G}_{ch}^1$ , the current flows in the same direction as the direction of the edges depicted, whereas, in  $\mathcal{G}_{dis}^2$ , the current flows in the opposite direction. Subsequently, regarding cell balancing, if  $v_1$  has a higher SoC than that of  $v_2$ , then the edge  $e_{12} \in E_{ch}^1$  will become active to transfer charge from  $v_1$  to  $v_2$  in  $\mathcal{G}_{ch}^1$ ; simultaneously,  $e_{21} \in E_{dis}^2$  will transfer charge from  $v_1$  to  $v_2$  in  $\mathcal{G}_{dis}^2$ , completing the cycle of charge transfer between cells.

Finally, this paragraph will provide the mathematical model of ACBN based on  $\mathcal{M}$ . In the first step, all the control efforts  $w_{i,j}^{ch}$  and  $w_{i,j}^{dis}$  are collected into weight matrices such that  $\mathcal{W}_{ch}^1 \subsetneq \mathcal{A}(\mathcal{G})_{ch}^1$ , and  $\mathcal{W}_{dis}^2 \subsetneq \mathcal{A}(\mathcal{G})_{dis}^2$ . In the similar fashion, as each edge in  $\mathcal{M}$  represents a charge transfer path, all the currents can be assembled into current matrices such that  $\mathcal{I}_{ch}^1 \subsetneq \mathcal{A}(\mathcal{G})_{ch}^1$ , and  $\mathcal{I}_{dis}^2 \subsetneq \mathcal{A}(\mathcal{G})_{dis}^2$ . Moreover, the expressions for the elements of  $\mathcal{I}_{ch}^1(i,j)$  and  $\mathcal{I}_{dis}^2(i,j)$ ,  $\forall i, j \in V$  and  $j = \{i \pm 1\}$ , are defined as follows:  $\mathcal{I}_{ch}^1(i,j) = I_{ch}(\mathcal{W}_{ch}^1(i,j), \mathcal{V}(v_i))$ , and  $\mathcal{I}_{dis}^2(i,j) = I_{dis}(\mathcal{W}_{dis}^2(j,i), \mathcal{V}(v_{i \pm 1}))$ , where  $\mathcal{V}(i)$  represents the open-circuit voltage of cell/vertex  $i$ . Therefore, the SoCs evolution of  $N$  cells based on the net currents and control actions are:

$$X_{k+1} = X_k + \frac{\delta T}{Q} (\mathcal{I}_{ch}^1 + \mathcal{I}_{dis}^2), \quad (2)$$

where  $X$  is a cell's SoC vector:  $X = [x_1, x_2, \dots, x_N]$ ,  $\delta T$  is time step, and  $Q$  is the cell's capacity. It is important to realize that current matrices, which dictate the dynamics of cells' SoCs in (2), derive their structure from  $\mathcal{A}(\mathcal{G})_{ch}^1$  and  $\mathcal{A}(\mathcal{G})_{dis}^2$  through the composition of functions. Consequently, encoding the ACBN topology using an adjacency matrix results in the appropriate allocations of the balancing currents to the designated cell. Similarly, as mentioned previously, the dynamics induced due to various components in the charge transfer paths are lumped into the edges of  $\mathcal{M}$ ; therefore, based on the suitable selection of the power electronic components, the relevant expressions for the balancing currents can be derived and incorporated accordingly. In this regard, the high-fidelity expressions for currents  $\mathcal{I}_{ch}^1(i,j)$  and  $\mathcal{I}_{dis}^2(i,j)$  are adapted from [16] and generalized as follows:

$$I_{ch}(i,j) = \frac{\mathcal{V}_h}{TR_{c_i}} \left( w_{i,j}T - t_d + \tau_{c_i} (e^{\kappa_i} - 1) \right), \quad (3)$$

$$I_{dis}(i,j) = \frac{\tau_{d_i} (e^{\chi_i} - 1)}{T} \left( -I_{p_i} - \frac{a_{0_i}(t_{0_i} - w_{i,j}T)}{\tau_{d_i} (e^{\chi_i} - 1)} + 1 \right), \quad (4)$$

$$t_{0_i} = w_{i,j}T + \tau_{d_i} \ln \left( \frac{R_{d_i} \mathcal{V}_h}{(\mathcal{V}_l + V_{F_{i,j}}) R_{c_i}} (1 - e^{\kappa_i}) + 1 \right),$$

$$\chi_i = \frac{w_{i,j}T - t_{0_i}}{\tau_{d_i}}, \quad a_{0_i} = \frac{\mathcal{V}_l + V_{F_{i,j}}}{R_{d_i}}.$$

$$I_{p_i} = \frac{\mathcal{V}_h}{R_{c_i}} \left( 1 - e^{\kappa_i} \right), \quad \kappa_i = \frac{t_d - w_{i,j}T}{\tau_{c_i}},$$

$$\lambda_i = \frac{t_d - t}{\tau_{c_i}}, \quad \phi_{i,j} = \frac{w_{i,j}T - t}{\tau_{d_i}}, \quad R_{d_i} = R_{0_l} + R_{\mathcal{L}_i},$$

$$R_{c_i} = R_{0_h} + R_{\mathcal{L}_i} + R_{ds}, \quad \tau_{c_i} = \mathcal{L}_i / R_{c_i}, \quad \tau_{d_i} = L_i / R_{d_i},$$

where higher and lower open circuit voltages are denoted by

$\mathcal{V}_h$  and  $\mathcal{V}_l$ , and their corresponding resistances ( $\Omega$ ) by  $R_{0_h}$  and  $R_{0_l}$  respectively; diode's  $D_{i,j}$  forward voltage is represented by  $V_{F_{i,j}}$ ;  $\tau_c$  and  $\tau_d$  are time constants (s) for charging and discharging of inductor  $i$ , respectively; inductor's peak current at  $t = u_{i,j}T$  is denoted by  $I_{p_i}$ ; dead time, switching time, and the time instant when inductor's currents become zero are denoted by  $t_d$ ,  $t_{0_i}$  and  $T$  respectively;  $u_{i,j}$  and  $\mathcal{L}_i$  represent duty cycle of  $S_{i,j}$  and inductance of inductor  $i$  (H), respectively; and  $R_{L_i}$ ,  $R_{ds}$ ,  $R_{c_i}$  and  $R_{d_i}$  represent resistances of inductor, on-state switching, and charging and discharging paths of inductor, respectively.

### III. NMPC FORMULATION FOR GRAPH-BASED ACBN

In this section, the NMPC problem is formulated for graph-based ACBN comprising  $N$  cells. By exploiting the fact that weight/control and current matrices borrow their structure from the adjacency matrix, the NMPC problem then naturally becomes scalable as depicted below. In the following, the cost function is designed to be balancing aware by declaring that all cells' SoC should converge to the pack's average SoC

$$\min_{x(k), w_{i,j}(k)} J(x(k), w_{i,j}(k)), \quad (5)$$

$$J = \sum_{k=k_0}^{k_0+H_p} \sum_{n=1}^N e_n^2(k),$$

$$e_n(k) = x_n(k) - \bar{x}(k), \quad \bar{x}(k) = \frac{1}{N} \sum_{n=1}^N x_n(k),$$

subject to

$$x(k+1) - f(x(k), \mathcal{W}(k)) = 0, \quad (5a)$$

$$X(k_0) = X_{k_0}, \quad (5b)$$

$$w_{i,j}(k) \in \mathcal{W}, \quad (5c)$$

$$x(k) \in \mathcal{X}, \quad (5d)$$

$$w_{i,j}(k).w_{j,i}(k) = 0, \quad (5e)$$

where  $H_p$  is the prediction horizon (s) with a value of 20 s;  $X_{k_0}$  is the initial state vector at the start of the optimization problem; and the sets  $\mathcal{W}$  and  $\mathcal{X}$  in (5c) and (5d), respectively, are given as:

$$\mathcal{W} = \left\{ w_{i,j} \in \mathbb{R}^+ \mid 0.1 \leq w_{i,j} \leq 0.4, \quad i \in V, \quad j = i \pm 1 \right\}, \quad (6)$$

$$\mathcal{X} = \left\{ x_n \in \mathbb{R}^+ \mid 0 \leq x_n \leq 1 \right\}. \quad (7)$$

The constraint in (5e) ensures that a given cell can't simultaneously give/receive charge to/from the same cell. Moreover,  $\mathcal{W}$  is used to represent either  $\mathcal{W}_{ch}^1$  or  $\mathcal{W}_{dis}^2$ , as the NMPC only needs to compute the efforts for a single layer of  $\mathcal{M}$  only.

#### A. Stability of Closed-loop system

Prior to demonstrating stability, it is important to validate that the total charge across the pack remains invariant under the suitable set of control actions. This is because the charge invariance property is part of the definition of the Lyapunov function—to be defined later, which in turn will be used to

demonstrate stability. Mathematically, the objective is then to show:  $\sum_{i=1}^N x_i(k+1) = \sum_{i=1}^N x_i(k)$ . This can be done by considering the state update equation (2):  $\sum_{i=1}^N x_i(k+1) = \sum_{i=1}^N x_i + \gamma \sum_{i=1}^N I_{\text{net}}(i)$ , where  $I_{\text{net}}(i) = \sum_{j=1}^N (\mathcal{I}_{ch}^1(i, j) + \mathcal{I}_{dis}^2(i, j))$ , and  $\gamma = \delta T/Q$ . Consequently,

$$\sum_{i=1}^N I_{\text{net}}(i) = \sum_{i=1}^N \sum_{j=1}^N (\mathcal{I}_{ch}^1(i, j) + \mathcal{I}_{dis}^2(i, j)), \quad (8)$$

where (8) is merely the summation of all elements in the matrix, including the diagonal and off-diagonal elements. Thus, the right-hand side of (8) can be rearranged as:  $\sum_{i=1}^N (\mathcal{I}_{ch}^1(i, i) + \mathcal{I}_{dis}^2(i, i)) + \sum_{\substack{i,j=1 \\ i \neq j}}^N (\mathcal{I}_{ch}^1(i, j) + \mathcal{I}_{dis}^2(i, j))$ , where the first term represents the summation along the diagonal terms and the second along the off-diagonal. Since in our definition of  $\mathcal{M}$ , there is no vertex that loops onto itself, the summation along diagonal terms is zero. Similarly, for off-diagonal terms, the control constraints (5e) and complementary weights imply that  $\forall i, j \in V, i \neq j : w_{ij}^{\text{ch}} = 0.4 \Rightarrow w_{ij}^{\text{dis}} \wedge w_{ji}^{\text{ch}} = 0.1$ , and vice versa. This—along with the assumption that charging and discharging currents have the same value—amounts to the fact that summation along the off-diagonal terms is zero as well. Therefore, the right-hand side of (8) is equal to zero. From the above steps, it is clear that:

$$\sum_{i=1}^N x_i(k+1) = \sum_{i=1}^N x_i(k) + \gamma \cdot 0 = \sum_{i=1}^N x_i(k) \square$$

To demonstrate the stability of ACBN comprising  $N$  cells, we utilize the dynamics—derived in Section II—and the constraints from the NMPC formulation, i.e., (5). By considering the following Lyapunov function

$$\mathcal{J} = \frac{1}{2} e^T e, \quad e^T = [e_1 \ e_2 \ \dots \ e_N], \quad (9)$$

its time derivative can then be given as

$$\begin{aligned} \dot{\mathcal{J}} &= \frac{1}{2} (e^\top \dot{e} + \dot{e}^\top e) = e_1 \dot{e}_1 + \sum_{n=2}^{N-1} e_n \dot{e}_n + e_N \dot{e}_N, \\ &= e_1 \dot{x}_1 + e_N \dot{x}_N + \sum_{n=2}^{N-1} e_n \dot{x}_n, \quad \because \sum_{n=1}^N e_n = 0, \\ &= \frac{e_1}{Q_1} (-I_{c_{1,1}} + I_{d_{1,2}}) + \frac{e_N}{Q_N} (-I_{c_{N-1,2}} + I_{d_{N-1,1}}) \\ &\quad + \sum_{n=2}^{N-1} \frac{e_n}{Q_n} (-I_{c_{n,1}} + I_{d_{n-1,1}} - I_{c_{n-1,2}} + I_{d_{n,2}}) - I_e \sum_{n=1}^N \frac{e_n}{Q_n}, \end{aligned} \quad (10)$$

To perform balancing, the NMPC-based control actuates the  $w_{i,j}$  while meeting the condition in (5e). Consequently, either the first or the second MOSFET of every BB converter will be turned on. For a battery pack containing a string of  $N$  cells, there are  $N^N$  possibilities of the relative magnitudes of cell's SoCs. Here, we will demonstrate the stability for two extreme cases: (i)  $x_1 > x_2 > \dots > x_N$ , and (ii)  $x_1 < x_2 < \dots < x_N$ . In case (i), only the upper edges in  $l = 1$  i.e.  $w_{ij}^{\text{ch}}$ ,  $\forall i, j \in V, j = i + 1$ , and similarly, the lower edges in  $l = 2$  will be

activated. Therefore, (10) can be expanded as follows:

$$\begin{aligned} \dot{\mathcal{J}} &= -I_e \left( \sum_{n=1}^{N/2} \frac{|e_n|}{Q_0 + \Delta Q_n} - \sum_{n=N/2}^N \frac{|e_n|}{Q_0 + \Delta Q_n} \right) \\ &\quad + \sum_{n=2}^{N/2} \frac{|e_n| (-I_{c_{n,1}} + I_{d_{n-1,1}})}{Q_0 + \Delta Q_n} - \sum_{n=N/2}^{N-1} \frac{|e_n| (-I_{c_{n,1}} + I_{d_{n-1,1}})}{Q_0 + \Delta Q_n} \\ &\quad - \frac{|e_1| I_{c_{1,1}}}{Q_0 + \Delta Q_1} - \frac{|e_N| I_{d_{N-1,1}}}{Q_0 + \Delta Q_N}. \end{aligned} \quad (11)$$

where  $Q_0$  is the nominal capacity of the cells and  $|\Delta Q_n| \leq 0.05$  is the perturbation term of each cell. The uncertainty in  $R_0$  only impacts the charging and discharging currents given by (3) and (4). In case of the nominal parameters the first three terms in (11) become 0 and  $\dot{\mathcal{J}}$  is negative. However, even for 5% and 10% uncertainties in  $Q_n$  and  $R_0$ , respectively, the last two terms in (11) dominate the time derivative of the Lyapunov functional, and its time derivative takes the following form

$$\dot{\mathcal{J}} \leq -\frac{|e_1| I_{c_{1,1}}}{Q_0 + \Delta Q_1} - \frac{|e_N| I_{d_{N-1,1}}}{Q_0 + \Delta Q_N}. \quad (12)$$

Which shows that  $\dot{\mathcal{J}}$  is negative definite and  $\mathcal{J}$  will eventually go to zero. Similarly, for the second case, the lower edges in  $l = 1$ , and upper edges in  $l = 2$  will be activated. Therefore, for this case, (10) can be expanded as follows:

$$\begin{aligned} \dot{\mathcal{J}} &= -I_e \left( \sum_{n=1}^{N/2} \frac{|e_n|}{Q_0 + \Delta Q_n} - \sum_{n=N/2}^N \frac{|e_n|}{Q_0 + \Delta Q_n} \right) \\ &\quad + \sum_{n=2}^{N/2} \frac{|e_n| (-I_{c_{n-1,2}} + I_{d_{n,2}})}{Q_0 + \Delta Q_n} - \sum_{n=N/2}^{N-1} \frac{|e_n| (-I_{c_{n-1,2}} + I_{d_{n,2}})}{Q_0 + \Delta Q_n} \\ &\quad - \frac{|e_1| I_{d_{1,2}}}{Q_0 + \Delta Q_1} - \frac{|e_N| I_{d_{N-1,2}}}{Q_0 + \Delta Q_N}. \end{aligned} \quad (13)$$

Like the previous case, if nominal parameters are considered, the first three terms in (13) become 0 and  $\dot{\mathcal{J}}$  is negative. Similarly, for 5% and 10% uncertainties in  $Q_n$  and  $R_0$ , respectively, the last two terms in (13) dominate and its derivative becomes:

$$\dot{\mathcal{J}} \leq -\frac{|e_1| I_{d_{1,2}}}{Q_0 + \Delta Q_1} - \frac{|e_N| I_{c_{N-1,2}}}{Q_0 + \Delta Q_N}. \quad (14)$$

Moreover, the same line of reasoning can be provided for any distribution of initial SoCs.

#### IV. RESULTS AND DISCUSSION

In the previous section, the closed-loop BB-converter-based ACBN was modeled in a scalable and modular fashion. In this section, the results of ACB under the NMPC framework will be discussed. Though the system-level manifestation of ACB will be quantified using EV range extension, the current modeling approach is equally applicable in evaluating other physical modules such as battery thermal regulation and health, etc. Moreover, the performance of NMPC will also be compared with a rule-based (RB) control strategy. The closed-loop scheme is depicted in Figure 2, wherein the central block represents the ACBN, comprising the battery pack and the BB converters.  $I_e$  represents the battery current

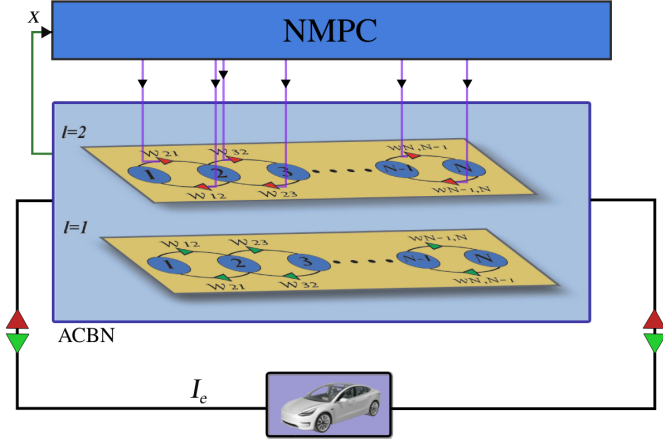


**Fig. 2:** NMPC implementation scheme for graph-based ACBN.

as demanded by the EV's powertrain. The NMPC takes in the information of SoCs of all cells and subsequently generates the duty cycles  $w_{i,j}$ . Moreover, the controller only computes  $w_{i,j}^{dis}$  as  $w_{i,j}^{ch}$  and  $w_{i,j}^{dis}$  are complementary, and only one of them needs to be computed. Although the NMPC problem is formulated for  $N$  cells, twelve cells are considered for the simulation purposes. This number represents the case study for the electric bike, whose voltage requirement of up to 40 V can be provided by 12 serially connected cells. Consequently, the power requirements for a specific application can also be scaled down accordingly. In this regard, LG 18650HG2 cell (cf. [17]) is considered for simulation, and its parameters along with the nominal values of ACBN are given in Table I.

**TABLE I:** Nominal model parameters for simulations

Parameter	Value	Parameter	Value
$T$	$20 \mu s$	$t_d$	$2 \mu s$
$V_F$	0.3 V	$R_{ds}$	$5.3 \text{ m}\Omega$
$t_f$	8 ns	$t_{rr}$	28 ns
$R_L$	$0.01 \Omega$	$L$	$6 \mu H$
$R_{0i}$	$0.025 \Omega$	$Q_{nom}$	10800 As

To evaluate the performance of ACBN for EV's range extension, realistic scenarios are considered by incorporating 7 different drive cycles—denoted as  $I_e$  in Figure 2:  $\mathcal{D} = \{\text{US06 City } (\mathcal{D}_1), \text{ US06 } (\mathcal{D}_2), \text{ US06 Highway } (\mathcal{D}_3), \text{ FHDS } (\mathcal{D}_4), \text{ FUDS Fast } (\mathcal{D}_5), \text{ FUDS } (\mathcal{D}_6), \text{ NEDC } (\mathcal{D}_7)\}$ . Similarly, up to 5% and 10% variations in capacity ( $Q$ ) and  $R_0$ , respectively are considered in the ACBS, whereas, the NMPC model considers the nominal parameters to showcase its robustness against parametric variations. Moreover, for each drive cycle, the range is calculated using the following: Range =  $\int_0^{t_{sim}} v_{DC}(t) dt$ , where  $v_{DC}$  is the velocity profile of drive cycles, and  $t_{sim}$  is the time instant when the SoC of any battery cell reaches 10%. Consequently, the range extension is then quantified by taking the difference of ranges achieved by ACB and no-balancing (NB) scenarios. Moreover, the balancing time ( $t_b$ ) is the time when the standard deviation of the SoCs  $\sigma(X(k)) = 0.02$ . The NMPC problem as formulated

in 5 was solved in MATLAB/Simulink using the CasADi toolbox and interior point optimizer (Ipopt) algorithm, with the sampling time of 10 s and the convergence tolerance of 1e-8. The simulations were performed on a computer with an Intel Core i7-1065G7, 1.3 GHz, 10<sup>th</sup> generation processor; 16 GB RAM; running Windows 11 Home (64-bit). Moreover, under the above condition, the average time to solve an optimization problem at each sampling time was 0.04 s. Regarding the NMPC computational complexity induced by the graph-based scalable model, it is worth mentioning that it increases as the number of cells grows. However, it doesn't depend on the way the system is modeled; rather it primarily depends on the system's dimension, NMPC parameters, solver settings, etc.

In the rest of the section, the performance metrics achieved by NMPC-based ACB will be discussed, and the comparison will be drawn with RB-ACB. For simulations, the vector of initial SoC levels is  $X^\top(0) = [65 \ 62 \ 85 \ 79 \ 75 \ 63 \ 77 \ 71 \ 82 \ 88 \ 76 \ 68]$ . Figure 3 demonstrates the results of ACB for the US06 Highway drive cycle—depicted in Figure 3c. It can be observed in Figure 3a that the pack started with an imbalanced SoC state. However, under the NMPC control actions, the states reached the equalized level in under 1 hour despite the aggressive demand of  $I_e$ . Once this state was achieved, the cells remained balanced for the rest of the drive cycle, and the balancing currents approached zero; cf. Figure 3b. Since NMPC generates 22 control signals for 12 cells, the net balancing currents—which are relatively fewer in number—are given in the results for better understanding. Moreover, it can also be observed that balancing currents are well within their specified bounds and the switching condition, i.e., (5e), is respected throughout the simulation.

Finally, Figure 4 shows the range achieved by NMPC, RB, and NB scenarios for all the drive cycles. The figure clearly shows that for each case, the range achieved by NMPC is higher than both RB and NB, with maximum range extensions of 38 and 42 km reported for FUDS and NEDC drive cycles, respectively. Overall, an average of 32 km range extension is achieved across all drive cycles. In comparison to RB, NMPC achieved a maximum range difference of 42 km in NEDC and a minimum difference of 5.5 km in US06HW. Table II better explains the variations in performance of both approaches by reporting the  $t_b$  and root mean square (RMS) of the control actions. In every scenario, NMPC balances more quickly than RB; therefore, the battery pack gets a longer operational time, which results in more range. Moreover, the RMS of RB is always greater than NMPC for all drive cycles. This is because RB makes the control decisions solely based on current SoC levels without any working knowledge of the system's dynamics. This results in transferring the same amount of charge among cells at each time step, and the controller keeps generating the control efforts even when the balancing criterion is met. Consequently, higher RMS and  $t_b$  result in lower range extension for RB-based ACB.

## V. CONCLUSIONS

In this work a variant of a graph, namely multiplex, is utilized to model a BB converter-based ACBN. The network

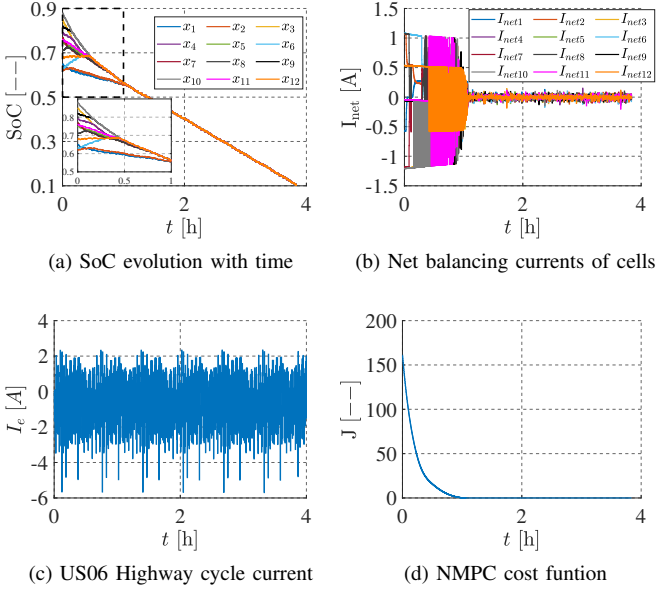


Fig. 3: ACBN performance under NMPC-based ACB.

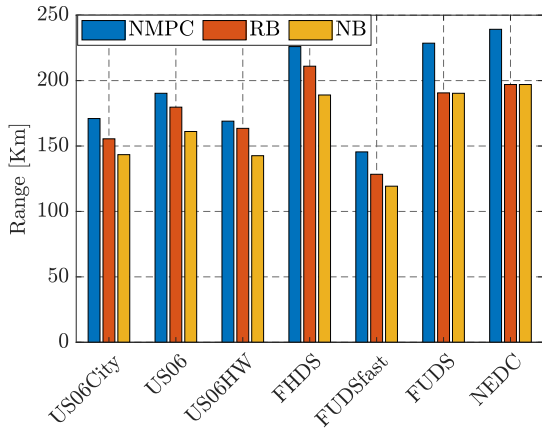


Fig. 4: Range extension across various drive cycles.

comprises  $N$  serially connected cells in adjacent-based cell-cell topology. The model is then brought under the NMPC framework to perform cell balancing to enhance the EV's range. The graph-based framework is important as it offers the flexibility to seamlessly capture the different ACBN topologies and architectures. This is delineated by the modeling process of BB converter-based ACBN and further integrating high-fidelity balancing currents to the graph structure. Moreover, the stability argument for the closed-loop system containing  $N$  cells is provided. The simulations were performed for a range of real-life driving scenarios, and the results demonstrated an average increase of 32 km in the EV's range.

The future work includes increasing the fidelity of the current graph-based model by incorporating the ACBN power losses and associating more physics modules such as thermal properties and aging, etc. This will pave the way to provide an exhaustive comparison of various ACBN types, including C2P/P2C, etc.

TABLE II: Balancing time and Root Mean Square of control actions of NMPC and RB controller

Drive Cycle	$u_{RMS}[\text{RB}]$	$u_{RMS}[\text{NMPC}]$	$t_b[\text{RB}]$	$t_b[\text{NMPC}]$
$\mathcal{D}_1$	0.2915	0.18	2320	2240
$\mathcal{D}_2$	0.2915	0.21	2310	2260
$\mathcal{D}_3$	0.2915	0.24	2300	2270
$\mathcal{D}_4$	0.2915	0.19	2310	2250
$\mathcal{D}_5$	0.2915	0.17	2320	2230
$\mathcal{D}_6$	0.2915	0.15	2330	2230
$\mathcal{D}_7$	0.2915	0.14	2330	2220

## REFERENCES

- [1] H. Li, C. A. Ooi, Z. Jia, K. Ammar, and M. K. Ishak, "A review of active cell balancing methods in electric vehicles," *Energy Conversion and Management: X*, vol. 28, p. 101244, 2025.
- [2] N. Ghaeminezhad, Q. Ouyang, X. Hu, G. Xu, and Z. Wang, "Active cell equalization topologies analysis for battery packs: A systematic review," *IEEE Transactions on Power Electronics*, vol. 36, p. 9119–9135, Feb 2021.
- [3] X. Cao, Q.-C. Zhong, Y.-C. Qiao, and Z.-Q. Deng, "Multilayer modular balancing strategy for individual cells in a battery pack," *IEEE Transactions on Energy Conversion*, vol. 33, p. 526–536, Jun 2018.
- [4] S. Wang, S. Yang, W. Yang, and Y. Wang, "A new kind of balancing circuit with multiple equalization modes for serially connected battery pack," *IEEE Transactions on Industrial Electronics*, p. 1–1, Jan 2020.
- [5] H. Chen, L. Zhang, and Y. Han, "System-theoretic analysis of a class of battery equalization systems: Mathematical modeling and performance evaluation," *IEEE Transactions on Vehicular Technology*, vol. 64, no. 4, pp. 1445–1457, 2015.
- [6] M. Negm, M. Morales, and W. Lynch, "Component evaluation and pspice modeling for charge pump based cell voltage balancer development," in *2021 IEEE Electric Ship Technologies Symposium (ESTS)*, pp. 1–7, 2021.
- [7] M. Caspar, T. Eiler, and S. Hohmann, "Systematic comparison of active balancing: A model-based quantitative analysis," *IEEE Transactions on Vehicular Technology*, vol. 67, no. 2, pp. 920–934, 2018.
- [8] Z. Zhang, L. Zhang, L. Hu, and C. Huang, "Active cell balancing of lithium-ion battery pack based on average state of charge," *International Journal of Energy Research*, vol. 44, no. 4, pp. 2535–2548, 2020.
- [9] Y. Chen, X. Liu, H. K. Fathy, J. Zou, and S. Yang, "A graph-theoretic framework for analyzing the speeds and efficiencies of battery pack equalization circuits," *International Journal of Electrical Power & Energy Systems*, vol. 98, pp. 85–99, 2018.
- [10] G. Dong, F. Yang, K.-L. Tsui, and C. Zou, "Active balancing of lithium-ion batteries using graph theory and a-star search algorithm," *IEEE Transactions on Industrial Informatics*, vol. 17, no. 4, pp. 2587–2599, 2021.
- [11] C. Yang, X. Zhang, C. Yang, L. Xin, H. Liu, and Y. Li, "Double-layer balance system of voltage source series energy storage battery pack for electric vehicles," *AIP Advances*, vol. 12, p. 025006, 02 2022.
- [12] Q. Ouyang, N. Ghaeminezhad, Y. Li, T. Wik, and C. Zou, "A unified model for active battery equalization systems," *IEEE Transactions on Control Systems Technology*, vol. 33, p. 685–699, Mar 2025.
- [13] M. Azmat Ullah, A. Ahmed, A. A. Uppal, and Q. Ahmed, "Nmpc-based performance evaluation of active balancing networks of li-ion batteries for overnight ev charging," *IEEE Access*, vol. 13, pp. 136016–136026, 2025.
- [14] F. Hoekstra, L. W. Ribelles, H. Bergveld, and M. Donkers, "Real-time range maximisation of electric vehicles through active cell balancing using model-predictive control," *2022 American Control Conference (ACC)*, p. 2219–2224, Jul 2020.
- [15] J. Chen, A. Behal, and C. Li, "Active cell balancing by model predictive control for real time range extension," *2021 60th IEEE Conference on Decision and Control (CDC)*, p. 271–276, Dec 2021.
- [16] S. B. Javed, A. A. Uppal, M. R. Azam, and Q. Ahmed, "Model-based quantitative analysis of power losses aware active cell balancing networks with load," *IEEE Transactions on Transportation Electrification*, pp. 1–1, 2024.
- [17] N. Campagna, V. Castiglia, R. Miceli, R. A. Mastromarco, C. Spataro, M. Trapanese, and F. Viola, "Battery models for battery powered applications: A comparative study," *Energies*, vol. 13, no. 16, 2020.